Complex Systems **2** (1988) 45–58

Lattice Gas Automata of Fluid Dynamics for Unsteady Flow

Hwa A. Lim
Supercomputer Computations Research Institute,
Florida State University, Tallahassee, Florida 32306-4052, USA

Abstract. We study lattice gas automata of fluid dynamics in the incompressible flow limit. It is shown that the viscosity effect on the transition layer from the steady uniform velocity in one stream to the steady uniform velocity in another, adjacent stream produces the correct profile. We further study the intrinsic damping or smoothing action of viscous diffusion and show that the results agree with those obtained from the Navier-Stokes equation. In both cases, we obtain a kinetic viscosity $\nu \sim 0.65$, consistent with the prediction of Boltzmann approximation.

1. Introduction

Cellular automata were originally introduced by von Neumann and Ulam [1] to study the behavior and the organization of very complex systems. Since, several attempts have been made among members of the physics community to find simple ways to describe and study the motion of a collection of interacting particles [2]. Notable among them are models of fluid motion [3–5]. In these models, time is discrete and particles collide in a lattice. On the theoretical side, it is known that real fluids are described by a set of so-called Navier-Stokes equations:

$$\frac{\partial \mathbf{u}}{\partial t} = -(\mathbf{u}.\nabla)\mathbf{u} - \nabla p + \nu \nabla^2 \mathbf{u}; \tag{1.1}$$

$$\nabla.\mathbf{u} = 0. \tag{1.2}$$

where $\mathbf{u}$ is the velocity, p is the pressure per unit mass density, and ν is the kinetic viscosity. The former is a statement of local momentum conservation while the latter is essentially an expression for local mass conservation. As will be seen later, these conservation laws are to be built into the lattice gas automaton if the model is to describe real fluids correctly.

The current impetus in these studies came with the recent advances in parallel computations. It is believed possible that such models, which belong

to a class of parallel computing systems with local rules known as cellular automata, may soon compete with the traditional computational methods [11]. Of particular interest is the use of binary arithmetic in this model instead of the high-precision arithmetic required by the conventional approach; moreover, complicated boundary conditions are more easily implemented. In this model, however, the Navier-Stokes equation is recovered only in the limit of large systems and for incompressible flows. More theoretical analysis remains to be done in order to bound the error of the lattice gas numerical scheme for finite lattice size and velocities [14]. It is the main aim of this paper to provide partial answers to this question by presenting numerical simulations of the dynamical behavior of the lattice gas and seeing how well the results compare with results of classical hydrodynamics.

We will study two examples in the unsteady unidirectional flow (see also [15]: the first is the interesting problem of smoothing-out of a discontinuity in velocity at a plane [7]. In the second, we study a problem that will be of particular interest for studying the motion in the boundary layer of periodic wave damped by friction. In either case, we show that the simulations generate the correct velocity profiles and the viscosity coefficient so extracted is in agreement with values obtained via other methods (e.g. Boltzmann approximation). In forthcoming papers [8,9], we will try to shed more light in this direction by studying flow patterns.

The paper is organized as follows. In section 2, we briefly discuss the model and define the various rules implemented into the model. Section 3 deals with the smoothing-out of discontinuity in velocity. The results and comparison with solutions of Navier-Stokes equation are presented in the same section. Section 4 presents the study of the boundary layer due to a vibrating plane and the results. The last section is reserved for conclusion.

2. The lattice gas automaton—model

The lattice gas model we use is that of Frisch, Hasslacher, and Pomeau [10]. At each site of the residing triangular lattice, particles can move in any of the six possible directions, $\mathbf{c_i}$, with i defined modulo six (see figure 1):

$$c_1 = \begin{pmatrix} \frac{1}{2} \\ \frac{\sqrt{3}}{2} \end{pmatrix} \tag{2.1}$$

$$c_2 = \begin{pmatrix} \frac{-1}{2} \\ \frac{\sqrt{3}}{2} \end{pmatrix} \tag{2.2}$$

$$c_3 = \begin{pmatrix} -1 \\ 0 \end{pmatrix} \tag{2.3}$$

$$c_4 = \begin{pmatrix} \frac{-1}{2} \\ \frac{-\sqrt{3}}{2} \end{pmatrix} \tag{2.4}$$

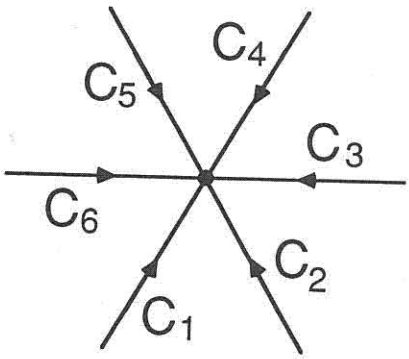

Figure 1: The six possible directions at each lattice site. At each site, no two particles can have the same velocity.

$$c_5 = \begin{pmatrix} \frac{1}{2} \\ \frac{-\sqrt{3}}{2} \end{pmatrix} \tag{2.5}$$

$$c_6 = \begin{pmatrix} 1 \\ 0 \end{pmatrix}. \tag{2.6}$$

There is, however, one stringent constraint on these velocities and this is usually referred to as the "exclusion principle". This principle states that *at any given site, no two particles can have the same velocity.* Taking this exclusion principle into account, a site may be empty or occupied up to a maximum of six particles. The evolution proceeds in two stages: at each time step, the particles propagate and then collide. During propagation, each particle moves one lattice constant in a direction determined by its momentum. Immediately following this, particles undergo collisions.

Our collision rules are *deterministic* so that the model is *chiral.* For symmetric two-particle head-on collisions with occupied input channels $(i, i+3)$, the occupied output channels are $(i+1, i+4)$. Figure 2 illustrates all possible two-particle collisions. It is obvious that this type of collision obeys conservation of momentum and conserves the particle number. However, careful observation reveals that there is also a spurious conservation—conservation of the difference in particle numbers in any pair of opposite directions $(i, i+3)$ [6]. This leads to conservation of four scalar quantities and the model would yield wrong macroscopic results unless this spurious conservation law is removed. A way to achieve this is to introduce symmetric three-particle collisions; with each occupied input channel $(i, i+2, i+4)$, the occupied output channel is $(i+1, i+3, i+5)$. Figure 3 depicts all possible such collisions.

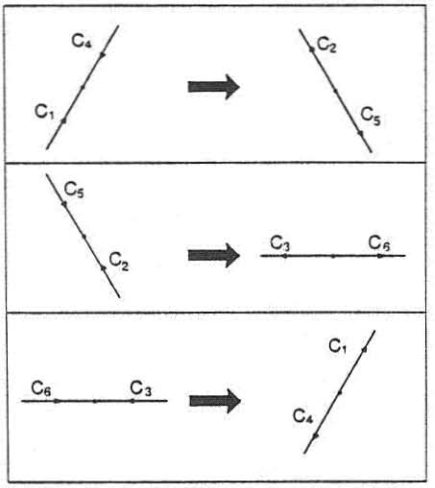

Figure 2: All possible two-particle collisions. A counter-clockwise rotation of 60° and so the collision rule is chiral.

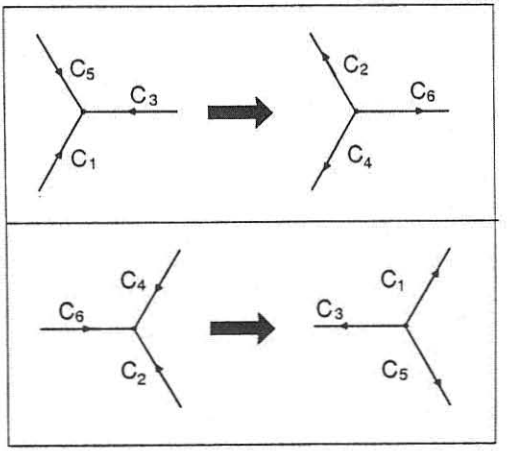

Figure 3: All possible three-particle collisions. A counter-clockwise rotation of 60°.

3. Smoothing-out of a discontinuity in velocity

We shall consider two adjacent streams moving with the same steady speed, but in opposite directions at time $t = 0$. If we denote the common speed of the streams at $t = 0$ by U and take the y-axis to lie along the transition layer, then with axes moving with the mean of the velocities of the streams, and a jump in velocity of $2U$ across the layer, the boundary conditions are:

$$u(x,0) = +U, \qquad x > 0; \tag{3.1}$$

$$u(x,0) = -U, \qquad x < 0. \tag{3.2}$$

In this situation, $u(x,t)$ will represent the excess velocity at position x at a subsequent time t.

3.1 Solution of Navier-Stokes equation

The solution of Navier-Stokes equation for the problem, with the above boundary conditions, has been solved and can be found in standard texts on fluid dynamics [7]. In terms of the only dimensionless combination of the pertinent physical parameters, the solution is:

$$\begin{aligned} u(x,t) &= \frac{U}{(\pi\nu t)^{\frac{1}{2}}} \int_0^x \exp(\frac{-x'^2}{4\nu t})\, dx' \\ &= U \operatorname{erf}(\frac{x}{(4\nu t)^{\frac{1}{2}}}). \end{aligned} \tag{3.3}$$

where $\operatorname{erf}(z)$ is the error function and is given by:

$$\operatorname{erf}(z) = \frac{2}{\sqrt{\pi}} \sum_{n=0}^{\infty} \frac{(-1)^n z^{2n+1}}{n!(2n+1)}. \tag{3.4}$$

3.2 Lattice-gas automaton simulation

In our simulation model, we have two streams of forced flows in the two halves of a 240 × 241 lattice. The stream flows are in the positive and negative y-directions. To mimic the infinite extent of the flow in the y-direction, periodic boundary conditions are imposed on the top (AA′) and bottom (BB′) of the lattice—c_1, c_2 on AA′ are mapped onto the corresponding sites on BB′; c_4, c_5 on BB′ are mapped onto the corresponding sites on AA′. The two walls (AB and A′B′) are taken to be specularly reflecting (see figure 4).

The flow is forced by adding momentum in the positive y-direction in the right half of the lattice, and by adding momentum in the negative y-direction in the remaining half of the lattice. This is achieved as follows: after each time step we randomly select a lattice site and apply, whenever allowed, one of the microscopic forcing rules described in Figure 5a and figure 5b. Each successful application of the forcing rule adds a unit of momentum to the stream. The forcing process is repeated until the desired amounts of momenta have been transferred to each stream [13]. This forcing process is

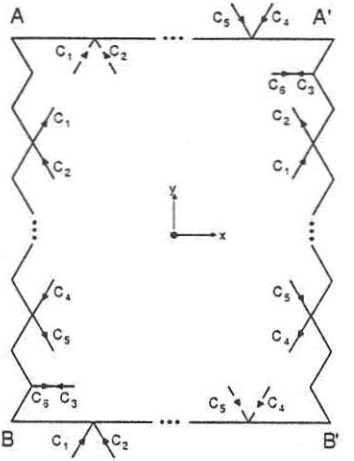

Figure 4: The lattice used for simulating flow of two adjacent streams. AA′ is mapped onto BB′ using periodic boundary condition; AB and A′B′ are specularly reflecting.

maintained until time step 6000, when the velocity profile has reached the stage corresponding to initial conditions as stated in equation (3.1,3.2). Then the forcing rule is "turned off". The net result of this is two adjacent streams of initial, equal speed U.

3.3 Results of lattice-gas automaton simulation

In the coarse-graining process, we divide BB′ into forty strips and AB into six rows [15]. The macroscopic mean density, ρ and macroscopic mean velocity, u are defined by [16]

$$\rho = \frac{2}{\sqrt{3}}\frac{1}{M}\sum_{i,\alpha}(N_i)_\alpha, \tag{3.5}$$

$$\rho u = \frac{2}{\sqrt{3}}\frac{1}{M}\sum_{i,\alpha}(N_i c_i)_\alpha, \tag{3.6}$$

where $i = 1,\ldots,6$, α sums over the sites enclosed in the region over which macroscopic means are taken, M is the total number of sites in the macroscopic region and is 6×40 in this example, $(N_i)_\alpha$ is the number of particles at site α with velocity c_i. The $\frac{2}{\sqrt{3}}$ factor arises because the residing lattice is triangular. With a total of 114153 particles in the 240×241 lattice, equation (3.5) gives $\rho = 0.37$.

We have checked that the mean density of gas does not vary significantly during the simulation and that the body forcing steps do not introduce appreciable lateral velocities. In fact, the mean density never varies more than 3% from its mean (0.37 ± 0.01) and the fluctuations in lateral velocity is less

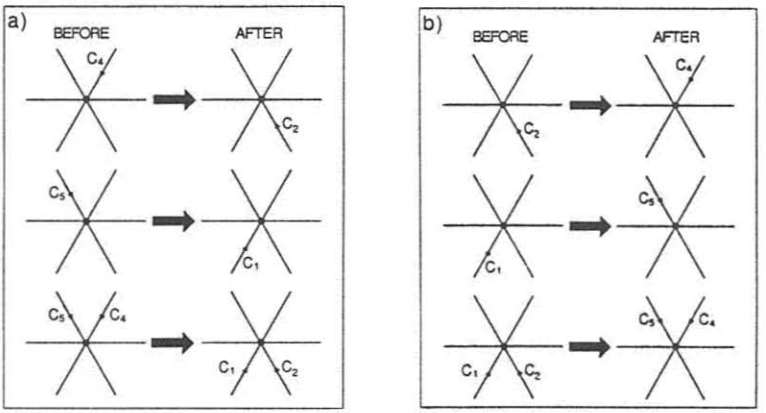

Figure 5: The forcing rules: (a) the three pairs of diagrams represent microscopic forcing rules to impart momentum in positive y-direction; (b) the corresponding microscopic forcing rules to impart momentum in the negative y-direction.

than 2% (0.0 ± 0.02). We have also carefully kept track of all the particles and made sure that no particles are lost or injected at each time step. These facts substantiate the simplification of equation (1.1) and the form of the solution, equation (3.3). A control simulation under the same conditions is run for 80000 time steps and it is observed that the maximum velocity attained approaches 0.7. This corresponds to U. In fact, this is also the maximum velocity at time step 6000. The mean velocity profiles at various times are shown in figure 6. It is seen that as time progresses, the width of the velocity profile at a fixed x becomes more and more narrow, in agreement with the prediction of equation (3.3). Figure 7 compares the simulation data points with the theoretically predicted form of equation (3.3). These graphs correspond to $t = 1000$ after the 'switch-off', and $\nu = 0.65$. They both seem to approach asymptotically to the value $u = 0.7$. It is seen that the two graphs agree very well for small u and the numerical data points deviate from the theoretical curve for $|u(x,t)| \geq 0.5$. This is very reminiscent of what has been observed in reference 14. In [14], it is noted that a characteristic feature of lattice gas automata is the appearance of higher-order corrections to the Navier-Stokes equations. These corrections are artifacts of the discrete nature of the lattice and they break Galilean invariance as soon as the ratio of the fluid velocity to the sound velocity (the Mach number) approaches unity. This may account for the deviations. In what follows, the fluid velocity considered is kept well below the sound velocity (0.707 in this model) to minimize these effects. For small argument of the error function, the solution takes the form (see also equation (3.4)):

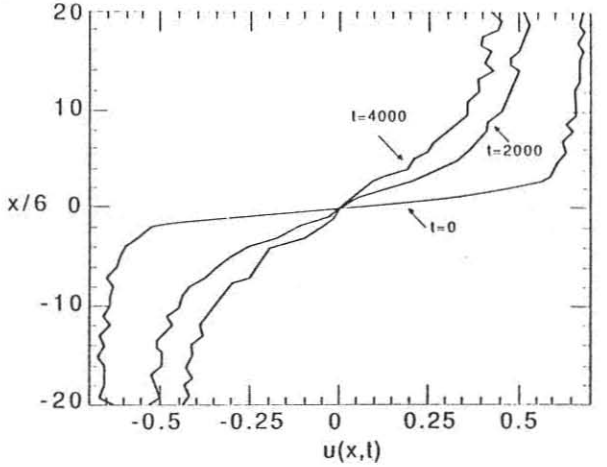

Figure 6: The velocity profiles of smoothing-out of a discontinuity in velocity at $t = 0$, $t = 2000$, and $t = 4000$ after the switch-off. Note that as time progresses, the profile narrows in.

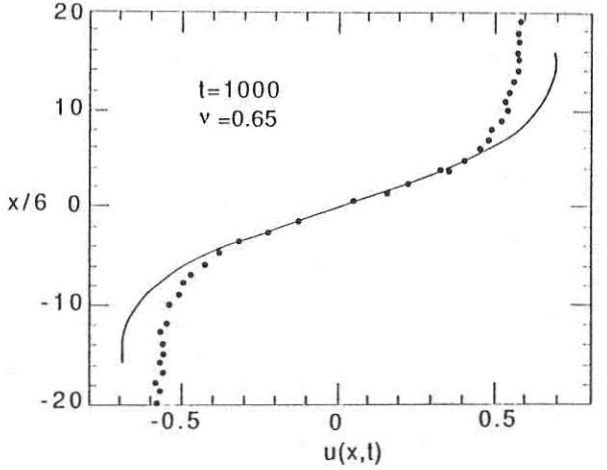

Figure 7: The velocity profile at $t = 1000$. The solid line is the theoretical prediction of Navier-Stokes equation. The profile is linear in the vicinity of the origin.

$\frac{\partial u}{\partial x} \sim 0.470 \times t^{-\frac{1}{2}} + 10^{-4}$	
t	$\frac{\partial u}{\partial x}$
500	0.0208
1000	0.0154
1500	0.0123
2000	0.0107
2500	0.0096
3000	0.0085

Table 1: Smoothing-out of a discontinuity in velocity. The slope for small arguments of the error function and the corresponding time.

$$u(x,t) \simeq \frac{2U}{\sqrt{\pi}} \frac{x}{(4\nu t)^{\frac{1}{2}}}. \tag{3.7}$$

From the form of equation (3.7) it is very tempting to fit the velocity profile with respect to the similarity variable $\frac{x}{\sqrt{t}}$ and leave ν as the regression coefficient. From the way the data are taken however, it is more appropriate to extract the viscosity from the gradient of the velocity profile close to the origin at various times. This is tabulated in table 1 and displayed in figure 8. From the linear fit of figure 8, we obtain

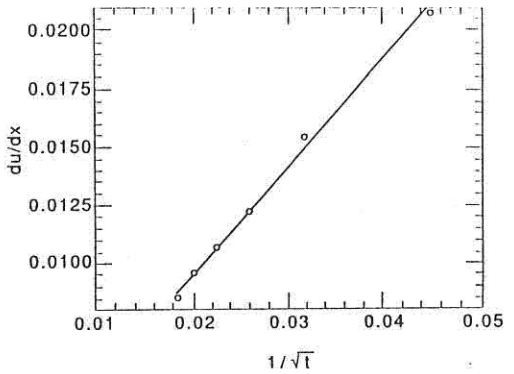

Figure 8: The slopes in the neighborhood of the origin at various times. The solid line is a linear fit.

$$\begin{aligned} \frac{2}{\sqrt{\pi}} \frac{U}{(4\nu)^{\frac{1}{2}}} &= 0.470 \\ \nu &\approx 0.70. \end{aligned} \tag{3.8}$$

This is to be compared with that obtained from Boltzmann approximation [14,17],

$$\nu_B = \frac{1}{12\rho}\frac{1}{(1-\rho)^3} - \frac{1}{8} \simeq 0.77, \tag{3.9}$$

where $\rho = 0.37$.

The two numbers are in good agreement, if we recall Boltzmann approximation always yields ν about 10% too high [6].

4. Flow due to an oscillating plane boundary

In this example, we shall consider a boundary moving sinusoidally in its own plane with velocity $u(0,t) = U\cos(\omega t)$ where ω is the angular frequency and U is the amplitude.

4.1 Solution of Navier-Stokes equation

The governing equation and boundary conditions of this example are [7]:

$$\frac{\partial u(x,t)}{\partial t} = \nu\frac{\partial^2 u(x,t)}{\partial x^2}, \tag{4.1}$$

$$u(0,t) = U\cos(\omega t), \tag{4.2}$$

$$u(\infty,t) = 0. \tag{4.3}$$

The solution of this equation, as can easily be verified by direct differentiation and substitution, is:

$$u(x,t) = U\exp\Big[-(\frac{\omega}{2\nu})^{\frac{1}{2}}x\Big]\cos\Big[\omega t - (\frac{\omega}{2\nu})^{\frac{1}{2}}x\Big]. \tag{4.4}$$

The velocity profile has the form of a damped harmonic oscillator with amplitude that decays exponentially with distance from the vibrating plane.

4.2 Lattice-gas automaton simulation

In this simulation model, the boundary conditions on the walls are as in section 3.2. The residing lattice is 80×1001 and is populated by 125015 particles. The flow is forced using the same technique as that of section 3.2, except the following differences:

(i) the forcing is performed only in the first strip ($x = 1 \rightarrow 10$),

(ii) the momenta are added in the positive or negative y-directions depending on the sign of $\cos\omega t$,

(iii) the amount of momenta added is not fixed. Rather, at each time step, it is equal to some constant amplitude multiplied by $|\cos\omega t|$.

The net result of these steps is that we have a left plane vibrating at an angular frequency of ω with amplitude U as shown in figure 9.

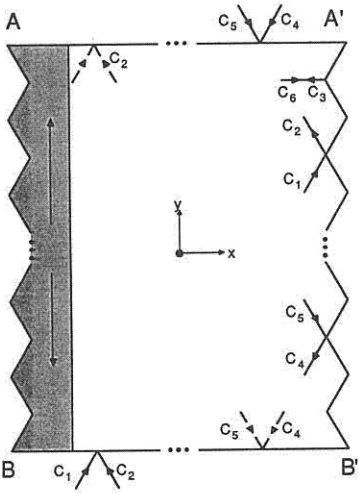

Figure 9: The lattice used for simulating flow due to a vibrating plane. AA′ and BB′ are mapped onto each other periodically; AB and A′B′ are specularly reflecting. Forcing rules are applied only in the first strip as described in the text.

4.3 Results of lattice-gas automaton simulation

In the coarse-graining process, we divide AA′ into ten strips and AB into twenty-five rows [14,15]. Since the fluid motion is set up from rest, the velocity profile contains transients. The velocity profiles shown in figure 10 are taken from time steps 320, 820, 1320 and 1820, after the transients have died away. These plots correspond to the velocity profiles at $t = \frac{0}{4}\tau$, $t = \frac{1}{4}\tau$, $t = \frac{2}{4}\tau$ and $t = \frac{3}{4}\tau$ respectively, where $\tau = 2000$ is the period. It is observed that the velocity profiles are harmonic functions of the time, with the same frequency ($\omega = \frac{2\pi}{2000}$) as that of the forcing vibrating plane just as predicted in equation (4.4)!

To extract the viscosity, we note that the velocity profile first crosses the $u = 0$ axis when the argument of the sinusoidal factor in equation (4.4) vanishes. This happens at ($t = 0$)

$$\left(\frac{\omega}{2\nu}\right)^{\frac{1}{2}} x - \omega t = \frac{\pi}{2}, \tag{4.5}$$

$$x^2 = \left(\frac{\pi}{4}\nu\right)\tau. \tag{4.6}$$

We tabulate in table 2 the positions of first zeroes for various periods and figure 11 is a plot of x^2 versus τ, the period. From the linear fit, we obtain,

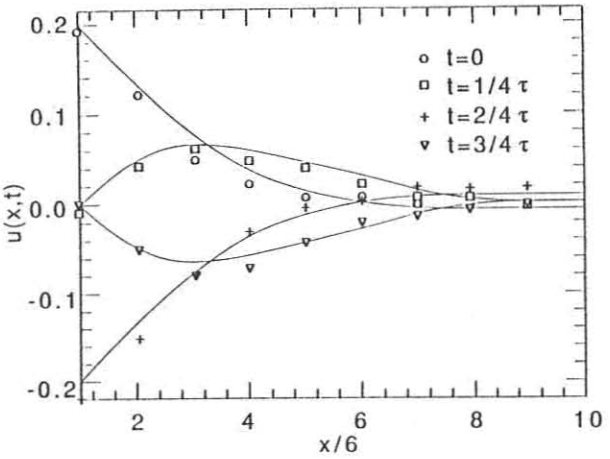

Figure 10: The velocity profiles set up by a vibrating plate at $t = 0$, $t = \frac{\tau}{4}$, $t = \frac{\tau}{2}$ and $t = \frac{3}{4}\tau$. The solid curves are theoretical predictions. The flow vibrates with the same frequency as that of the forcing plate.

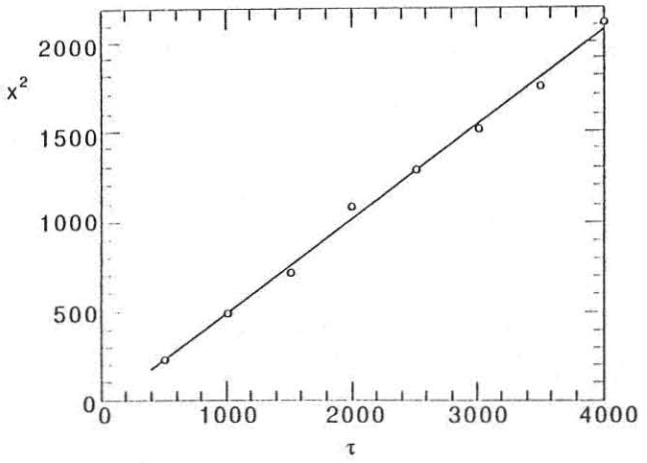

Figure 11: A plot of the distances squared from the vibrating plate of first zeroes versus the periods. The solid line is a linear fit.

Linear regression		$x^2 \sim 0.529 \times \tau - 37.0$		
Linear regression		$\log(A) = 0.62 \times \log(\tau) - 2.78$		
A	t	x	x^2	τ
0.08	100	15	225	500
0.12	200	22	484	1000
0.15	240	27	729	1500
0.19	320	33	1089	2000
0.22	420	36	1296	2500
0.24	580	39	1521	3000
0.27	660	42	1764	3500
0.28	680	46	2116	4000

Table 2: Flow due to an oscillating plane. Response amplitudes, time, position of first zeroes and the vibrating periods.

$$\frac{\pi}{4}\nu = 0.529. \tag{4.7}$$

or that $\nu \approx 0.67$ which is again in agreement with that of equation (3.9) ($\rho = 0.30, \nu_B \simeq 0.70$). It is also interesting to note that the response amplitudes seem to obey a power law of the form $A \sim \tau^{\frac{3}{5}}$ for a fixed vibrating plate amplitude.

5. Conclusion

We have shown, by simulating two interesting and important examples from incompressible fluid dynamics, that the lattice-gas automata are capable of producing results which are consistent with classical hydrodynamics. Though these examples provide no rigorous proof that lattice-gas automata can compete with traditional computational methods in efficiency, they do show that lattice-gas automata, with certain restrictions, may be a viable alternative for solutions of fluid dynamics. This is especially true when very complicated boundary conditions are to be implemented.

Acknowledgements

The author would like to thank Dr. D. Schvartz who introduced him to the subject. Assistance from D. Kakarigi, the Supercomputer Computations Research Institute staff is fully acknowledged and encouragement from Prof. R. R. Whitehead is appreciated.

The author is also grateful to the Laboratory for Laser Energetics for the use of the CYBER 180/990, DISSPLA facilities; SCRI for the use of the CYBER 205. This work is partially supported by US Department of Energy under the contract number DE-FC05-85ER250000.

References

[1] J. von Neumann, *Theory of Self-Reproducing Automata*, (University of Illinois Press, 1966).

[2] I.E. Broadwell, *Phys. of Fluids*, **7** (1964) 1243; R. Gatignol, "Théorie Cinétique des Gaz à Répartition Discrète de Vitesse," *Lecture Notes in Physics* (Springer-Verlag, Berlin, 1975).

[3] J. Hardy and Y. Pomeau, *J. Math. Phys.*, **13** (1972) 1042.

[4] J. Hardy, O. de Pazzis and Y. Pomeau, *J. Math. Phys.*, *14* (1973) 1746.

[5] J. Hardy, O. de Pazzis and Y. Pomeau, *Phys. Rev.*, **A13** (1976) 1949.

[6] U. Frisch, D. d'Humières, B. Hasslacher, P. Lallemand, Y. Pomeau and J. P. Rivet, *Complex Systems*, **1** (1987) 649.

[7] G. K. Batchelor, *An Introduction to Fluid Dynamics* (Cambridge Univ. Press, Cambridge, England, 1967).

[8] G. Riccardi, H. A. Lim and C. Bauer, *A Vectorized Cellular Automata Model of Fluid Flow*, in preparation.

[9] H. A. Lim, G. Riccardi and C. Bauer, *Applications of Cellular Models to Flow Patterns*, in preparation.

[10] U. Frisch, B. Hasslacher and Y. Pomeau, *Phys. Rev. Lett.*, **56** (1986) 1505.

[11] *Complex Systems*, **1** (1987) G. Doolen.

[12] S. Wolfram, *Theory and Applications of Cellular Automata* (World Scientific Publishing Co., Singapore, 1986).

[13] L. P. Kadanoff, G. R. McNamara and G. Zanetti, *Complex Systems* **1** (1987) 791.

[14] F. Hayot, *Complex Systems* **1** (1987) 753.

[15] F. Hayot, *Phys. Rev.* **A35** (1987) 1774.

[16] K. Balasubramanian, F. Hayot and W. F. Saam, *Phys. Rev.* **A36** (1987) 2248.

[17] J. P. Rivet, U. Frisch, *Comptes rendus* **302**, *série 11* (1986) 267